Atmos. Chem. Phys. Discuss., 10, 17657–17697, 2010
www.atmos-chem-phys-discuss.net/10/17657/2010/
doi:10.5194/acpd-10-17657-2010

Atmospheric Chemistry and Physics Discussions

Comparison of global inventories of monthly CO emissions derived from remotely sensed data

D. Stroppiana[1], P. A. Brivio[1], J.-M. Grégoire[2], C. Liousse[3], B. Guillaume[3], C. Granier[4,5,6], A. Mieville[4], M. Chin[5], and G. Pétron[6,7]

[1]CNR, Istituto per il Rilevamento Elettromagnetico dell'Ambiente, Milano, Italy
[2]EC, Joint Research Centre, Varese, Italy
[3]Laboratoire d'Aérologie, Toulouse, France
[4]Service d'Aéronomie/CNRS, Paris, France
[5]NASA/Goddard Space Flight Center, Greenbelt, MD, USA
[6]NOAA Global Monitoring Division, Earth System Research Laboratory, Boulder, CO, USA
[7]University of Colorado, Cooperative Institute for Research in Environmental Sciences, Boulder, CO, USA

Received: 6 July 2010 – Accepted: 12 July 2010 – Published: 22 July 2010

Correspondence to: D. Stroppiana (stroppiana.d@irea.cnr.it)

Published by Copernicus Publications on behalf of the European Geosciences Union.

Abstract

Five global inventories of monthly CO emissions named VGT, ATSR, MODIS, GFED2 and MOPITT and based on remotely sensed active fires and/or burned area products for the year 2003 are compared. The objective is to highlight similarities and differences focusing on the geographical and temporal distribution of the emissions at the global and continental scale and for three broad land cover classes (forest, savanna/grassland and agriculture). Emissions for the year 2003 range between 398 Tg CO and 1422 Tg CO. Africa shows the best agreement among the inventories both in terms of total annual amounts (162.4–367.4 Tg CO) and of seasonality despite some overestimation of emissions from forest and agriculture land covers observed in the MODIS inventory. Eurasian boreal forests most contribute to the large difference observed due to the high fuel loads involved in burning. In these regions VGT tends to overestimate emissions especially outside the typical fire season. In South America the perfect agreement of annual totals given by VGT and MOPITT (121 Tg CO) hides a different geographical distribution of CO sources: compensation effects between the 0.5° grid cells lead to a better agreement when looking at regional or annual totals. Looking at the broad land covers, the range of contribution to global emissions is 64–74%, 13–19% and 3–4% for forests, savanna/grasslands and agriculture, respectively. Results suggest that there is still large uncertainty in global estimates of emissions and attention should be paid to accurate parameterization of vegetation characteristics and conditions at the time of fire.

1 Introduction

Since the late 70s (Crutzen et al., 1979), prescribed and wild vegetation fires have been recognized as a major source of atmospheric trace gases and aerosol particles that affect the composition of the atmosphere and the global climate. Fires are a significant anthropogenic source of greenhouse gases (CO_2 and CH_4): deforestation and

ACPD
10, 17657–17697, 2010

changing agricultural practices have contributed 25% to the increase in CO_2 since pre-industrial time (IPCC, 2007). Other carbonaceous compounds are also emitted by the incomplete combustion of vegetation such as CO: CO_2 and CO are in fact responsible for 90–95% of the total carbon released by fires (Andreae and Merlet, 2001). According to IPCC (2001) about 40% of the CO annual budget in the atmosphere is due to fires and fires are responsible for almost all of its inter-annual variability (Novelli et al., 2003; van der Werf et al., 2004). For example, the 1997/1998 El Niño event has been linked to increased fires in the boreal regions and in the tropics and to a strong atmospheric CO anomaly (Langenfelds et al., 2002; Novelli et al., 2003; van der Werf et al., 2003). Moreover, CO is an important sink for hydroxyl radicals (OH) and it is a precursor of ozone (O_3) and for these reasons it plays a key role in chemical transport models of atmospheric pollutants (Jain, 2007).

The remaining fraction of total carbon emitted by fires (5%) is released as particulate matter (Reid et al., 2005). Even if lower in percent, these particles have a strong effect on the radiation budget. The aerosols released by the combustion process scatter and absorb incoming solar radiation and change the atmospheric radiation budget (Hobbs et al., 1997; Podgorny et al., 2003) besides their influence on cloud formation and on cloud microphysical processes (Langmann et al., 2009). Black carbon, which constitutes 5–10% of the particle emissions from fires (Liousse et al., 1996; Reid et al., 2005) and has a direct effect on absorbing radiation in the atmosphere, can also reduce albedo when deposited on snow and ice, thus inducing a positive radiative forcing (global warming). Also, land cover change, which is one of the main causes of vegetation fires, itself induces a change of surface albedo.

These are only some of the major and complex processes that impact on the global climate and have been discussed in a number of studies (Innes et al., 2000). Also, climate variability and change itself can influence fire frequency (Westerling et al., 2006). Finally, let us note that recent publications have also pointed out that fires can be a source of extremely toxic products such as mercury (Friedli et al., 2009).

Great uncertainty still exists in the assessment of gas and particulate emissions be-

ACPD
10, 17657–17697, 2010

cause of the higher temporal dynamic of vegetation fires with respect to other sources such as fossil fuel combustion (Liousse et al., 2004; Langmann et al., 2009); fires over the globe are in fact characterized by high variability from place to place and from year to year and by high seasonality (Anyamba et al., 2003; Hély et al., 2003; Boschetti et al., 2004; Michel et al., 2005). Remotely sensed data potentially have all the characteristics for quantifying seasonal and inter-annual information on the emissions from vegetation fires because of their global and quasi continuous coverage (Cooke et al., 1996; Generoso et al., 2003). Moreover, the high frequency with which satellite data are acquired is particularly suited for compounds such as CO since its average global lifetime in the atmosphere is about two months.

Two approaches have so far been developed to estimate CO emissions from fires. The *bottom-up* approach relies on the model provided by Seiler and Crutzen (1980) and has been widely applied at continental and global scales with various spaceborne sensors (Barbosa et al., 1999; Stroppiana et al., 2000; Conard et al., 2002; Schultz, 2002; Michel et al., 2005; van der Werf et al., 2006; Yan et al., 2006; Konare et al., 2008; Liousse et al., 2010). In this approach, estimates of the surface burned by fires is converted into emitted gases and aerosols with a multiplicative model of parameters which take into account the amount of biomass available for burning, the biomass actually burned by the fire and the amount of gases and aerosols emitted for each unit of burned biomass. These parameters are generally land cover type dependent.

From the late Nineties, inversion models have been developed to derive emissions from CO concentrations measured in the atmosphere (Manning et al., 1997; Bergamaschi et al., 2000; Pétron et al., 2002). Exploitation of remotely sensed concentrations of atmospheric gases is more recent and has rapidly increased with the use of the NASA-MOPITT (Measurements OF Pollution In The Troposphere) instrument (Pétron et al., 2004; Liu et al., 2005; Arellano et al., 2006; Chevallier et al., 2009). The latter is also known as *top-down* approach and consists of estimating carbon surface fluxes from the atmospheric concentrations.

Large differences in both the geographic distribution and temporal dynamics of global

ACPD
10, 17657–17697, 2010

and regional CO emission estimates are reported in literature; these differences are primarily due to uncertainties in the input data on burned area and fuel loads (Langmann et al., 2009) and in either modeling or inversion techniques (Pétron et al., 2004).

Recent developments in remote sensing have made global datasets of active fires and burned areas, which can be exploited for emission estimation, widely available. Active fire counts (the number of active fires per grid cell) have been used for a long time for depicting temporal and spatial patterns of vegetation fires (Cooke et al., 1996; Dwyer et al., 2000) as well as for quantifying the area burned (Giglio et al., 2006). Since active fire mapping relies on the detection of the high thermal emission from the flaming front of the fire, it is an important source of information for the detection of small events and of fires burning below dense canopies. However, active fire mapping is significantly affected by the presence of clouds at the time of observation and is a sample of the total daily fire activity. By integrating the perimeter of the area affected by the fire, the area burned product should provide a better quantification of the fires. Burned area mapping is less affected by could cover due to the persistence of the burned signal. However, burned area mapping can be rather difficult over large areas especially where the remotely sensed signal can be confused with other surface targets (e.g. low albedo surfaces such as shadows, water and some types of soil). Since neither active fire counts nor burned area mapping can provide a satisfying global picture of the geographical and temporal variability of vegetation fires, both are still used by the scientific community for emission estimation with many algorithms to combine the two products.

The objective of this paper is to present the comparison of five global inventories of monthly CO emissions from vegetation fires for the year 2003. In particular, we aim to highlight similarities and differences in the seasonality and in the geographical distribution of emissions at the global and continental levels and for three broad land cover types: forest, savanna/grassland and agriculture. Despite the numerous literature available about regional estimates, very few studies have attempted so far to compare global datasets of burned areas or pyrogenic emissions from fires and even fewer have specifically addressed the issue of comparing both spatial and temporal

ACPD
10, 17657–17697, 2010

distributions (Jain, 2007; Chang and Song, 2009). The inventories analysed here are derived from different fire burned area and/or active fire products and satellite sensors; four of them are based on a *bottom-up* approach while a fifth dataset is derived with a *top-down* approach which exploits the concentrations of atmospheric gases as measured by the MOPITT instrument and inverse modelling techniques. This last dataset can be assumed as an independent estimate which can help identifying limits of the *bottom-up* estimates (van der Werf et al., 2006). We also analyze the distribution of CO sources among forest, savanna/grassland and agriculture land cover classes for the VGT, ATSR and MODIS products. We focused on CO emissions because biomass burning is the major source of this chemical compound in the troposphere. Moreover, CO emissions are often used as a reference for the estimation of other pollutants during the combustion process (Andreae and Merlet, 2001).

2 Data and methods

The five CO inventories (Table 1) can be divided into three categories. In the first category, three inventories were built directly from recent global fire products derived from satellite time series which were processed to map either the occurrence of fire events or to map directly the area burned. Called VGT, ATSR and MODIS in this document, these inventories were derived using one common land cover map and a common set of biomass densities, burning efficiency coefficients and emission factors. The fourth inventory, called GFED2 in this document, was also derived from a satellite fire product but with a different set of data for the fuel load, burning efficiency and emission factors. The fifth inventory, called MOPITT, was derived from remote sensing CO observations coupled with an active fire dataset.

ACPD
10, 17657–17697, 2010

2.1 Global CO inventories

2.1.1 The VGT inventory

This inventory was built by the Centre National de la Recherche Scientifique-Laboratoire d'Aérologie (CNRS-LA) to derive gaseous and particulate emissions for the 2000–2007 period (Liousse et al., 2010). It is based on the L3JRC burned area product (Tansey et al., 2008) derived from the 1 km daily images of the Vegetation (VGT) sensor onboard the SPOT (Satellite Pour l'Observation de la Terre) satellites. Developed by a consortium of four European research institutions, the Universities of Leicester, Lisbon, Louvain-la-Neuve, and the European Commission Joint Research Centre (EC-JRC), this data set provides the area burned globally on a daily time step for seven years (2000 to 2007) at a resolution of 1 km. A further calibration was applied to the estimated burned area for the *deciduous broad-leaved tree* (GLC03) and the *deciduous shrub cover* (GLC12) land cover classes as derived from the Global Land Cover 2000 map (GLC2000) (Bartholomé and Belward, 2005). Corrections to the 1 km burned area map derived from L3JRC were based on the analysis of high resolution satellite data (Landsat Thematic Mapper). Monthly CO was estimated for each land cover type using the Biomass Density (BD [$kg\,m^{-2}$]), Burning Efficiency (BE [unitless]) and Emission Factor (EF [$g\,CO\,kg^{-1}$]) reported in Mieville et al. (2010) and Liousse et al. (2010).

2.1.2 The ATSR inventory

This global inventory was extracted from the Inventory for Chemistry Climate studies (GICC) produced by the CNRS-SA (Centre National de la Recherche Scientifique-Service d'Aéronomie) and CNRS-LA in the context of the ACCENT-GEIA program (http://www.accent-network.org/). Emissions of several chemical species from biomass burning for the period 1997–2005 have been quantified in three steps (Mieville et al., 2010). First, the Global Burnt Area 2000 (GBA2000) product was used to derive CO

ACPD
10, 17657–17697, 2010

emissions for the year 2000. GBA2000 was released by the EC-JRC in partnerships with eight research institutions (Grégoire et al., 2003) and provides the area burned globally, for each month of the year 2000, as derived from 1 km SPOT-VGT images (Tansey et al., 2004). The resulting emissions from BD, BE and EF described in Mieville et al., 2010 and Liousse et al., 2010 were re-gridded to a 0.5×0.5° resolution and used to calibrate, in terms of spatial and temporal distribution of CO emissions, the active fire counts contained in the World Fire Atlas (WFA) product developed by the European Space Agency (Arino and Plummer, 2001). The WFA provides the geographical location of night-time active fires, detected by the Along Track Scanning Radiometer (ATSR-2) sensor onboard the ERS-2 (European Remote Sensing) satellite, for the period 1995–2002, and by the Advanced Along Track Scanning Radiometer (AATSR) sensor onboard the ENVISAT platform since 2003 (http://dup.esrin.esa.it/ionia/wfa/index.asp). It must be noted that the WFA gives access to a long time series, but is restricted to night-time fire events and shows a relatively high level of false detection as demonstrated by Mota et al. (2005). The calibration was carried out separately for three latitudinal bands (−90° S to −15° S; −15° S to 15° N; 15° N to 90° N) based on the assumption that within the same latitudinal band and vegetation class all fire pixels of the WFA product represent the same average burned surface, and thus the same average emitted CO. Finally, the WFA time series of night-time fire counts was translated into CO emissions for the 1997–2005 period using the same set of coefficients as the VGT inventory.

2.1.3 The MODIS inventory

This inventory is based on the 8-day fire counts at 1-km resolution derived from the MODIS (Moderate Resolution Imaging Spectroradiometer) sensor onboard the Terra and Aqua satellites (Justice et al., 2002). It uses the Version 4 of the monthly Climate Modeling Grid (CMG) (NASA/University of Maryland, 2002) fire product at 0.5×0.5° resolution, from January 2001 to December 2004. The conversion factors proposed by Giglio et al. (2006) were used to build a set of monthly burnt area estimates for the year

ACPD
10, 17657–17697, 2010

2003 (Chin et al., 2002). The MODIS CO inventory was finally derived using the same coefficients as the VGT and ATSR inventories and reported in Mieville et al. (2010) and Liousse et al. (2010).

2.1.4 The GFED2 inventory

The Global Fire Emissions Database version 2 (GFED2), released at the beginning of 2006 (van der Werf et al., 2006), provides a range of data at 1×1° spatial resolution globally for the period 1997–2004: burned area, fuel load, combustion completeness and emissions from fires for a series of gases and aerosols. The inventory used in this study is composed of CO emissions at a monthly time step for the year 2003 computed from MODIS burned area time series derived from active fire counts (Giglio et al., 2006), fuel loads estimated by applying the satellite-driven CASA (Carnegie-Ames-Stanford-Approach) biogeochemical model, time-dependent combustion completeness and emissions factors proposed by Andreae and Merlet (2001). Although derived with the same *bottom-up* approach as the previous VGT, ASTR and MODIS inventories, van der Werf et al. (2006) state that this inventory better represents fire seasonality in boreal ecosystems and global wetland due to the improved modelling of fuel loads.

2.1.5 The MOPITT inventory

The MOPITT emission inventory is built using a *top down* model (Pétron et al., 2004). A set of a-priori sources of CO emissions (fossil fuel, biogenic fuel and vegetation fires from MODIS active fire counts) (Pétron, personal communication) is combined with the global chemistry and transport Model for OZone and Related chemical Tracers (MOZART; Horowitz et al., 2003), which simulates the distribution of 63 trace gases in the lower atmosphere, to relate surface to tropospheric emission perturbations. Inversion techniques are then applied to extract correction factors of the a-priori fluxes based on the minimization of the difference between tropospheric observed (MOPITT profiles binned onto the MOZART model 2.1×2.85° horizontal grid) and modelled CO.

ACPD
10, 17657–17697, 2010

Inversion is carried out for fifteen large regions over the globe. The dataset has been interpolated to a resolution of 0.5×0.5° to be consistent with the other datasets.

2.2 Inventory comparison

The five inventories were compared over the globe and six continental windows (North America: 180° W–50° E 75° N–30° N; Europe: 30° W–45° E 71° N–26° N; Northern Asia: 45° E–180° E 71° N–26° N; South America: 117° W–33° W 30° S–50° S; Africa: 30° W–63° E 26° N–50° S; Oceania: 63° E–180° E 26° N–50° S) (Boschetti et al., 2004). We first compared maps of annual CO and totals over geographical areas. Since annual totals hide compensation effects between the cell values summed up over the year and/or a window (Generoso et al., 2003), we also carried out cell by cell comparisons: we computed the coefficient of determination (R^2) by regressing all 0.5×0.5° cells (each cell value is the sum of the monthly 2003 values) of the geographical windows and the globe. We also performed a simultaneous comparison of seasonality and geographical agreement through regression of monthly 0.5° cell CO emissions for each of the VGT, ATSR, MODIS and GFED2 inventories against the MOPITT inventory. Following van der Werf et al. (2006), we assumed MOPITT as a reference dataset since the approach used to estimate emission is independent from the other approaches. We looked at the Pearson coefficient (r) and at the slope of the regression line (α): r quantifies the agreement in terms of seasonality and the slope quantifies the difference in terms of absolute values of CO emissions between the compared pairs; since a good correlation does not imply a small difference between the estimates, we attempted to combine these two information by creating eight classes describing the difference observed between the estimates provided by two inventories.

A further analysis was carried out only for the VGT, ATSR and MODIS estimates which were made available per land cover type: we looked at the distribution of emissions among three broad land covers derived by grouping the GLC2000 classes where fires occur: forest (GLC2000 classes 1, 2, 4, 5, 6, 9), savanna/grassland (GLC2000 classes 11 to 14) and agriculture (GLC2000 classes 16 to 18) (Mieville et al., 2010).

ACPD
10, 17657–17697, 2010

Vegetation characteristics, particularly the high variability of the amount of biomass available for burning, can in fact have a significant weight on the distribution of emissions in space and time (Michel et al., 2005).

3 Results and discussion

3.1 Geographical distribution of CO emissions

Table 2 shows total CO emissions estimated from the five inventories for 2003. The global amounts range from nearly 398 Tg (GFED2) to 1422 Tg (VGT), with VGT almost two times greater than the second largest value given by MODIS (769.6 Tg CO). The inventories compared in this study are within the range given by previous studies, except VGT. The GFED2 dataset gives for the period 1997–2004 a minimum for global CO emissions from vegetation fires of 337.6 Tg CO in 2000 and a maximum of 592.2 Tg CO in 1998 (van der Werf et al., 2006). According to IPCC (2001), the contribution from vegetation fires to the CO global budget ranges between 300 and 700 Tg CO/yr although this source is recognized as the most variable part of the CO budget. In all of the northern continents VGT are the highest estimates; in South America VGT and MOPITT coincide (121 Tg CO) and in Africa and Oceania MODIS provides the greatest values. With the exception of South America, GFED2 is the lowest of the inventories. As a reference for comparison, Liousse et al. (2010) built an emissions inventory for West Africa at the 1 by 1 km resolution by exploiting the L3JRC product and observed an overestimation of 45% when compared to GFED2.

The difference between the inventories is significant in North America and Europe (Coefficient of Variation CV=σ/μ above 145%) while smaller discrepancies are observed for the southern continental windows and in particular for Africa (162.4–367.4 Tg CO, CV=31%) and Oceania (57.9–92.60 Tg CO, CV=21%). These figures suggest that VGT overestimates CO emissions at the northernmost latitudes where any difference in burned area estimates is amplified by forest fuel loads that can be more

ACPD
10, 17657–17697, 2010

than 20 times greater than the savanna's and by forest vegetation composition (e.g. the fraction of tree cover) that can favor emissions of incomplete combustion products such as CO. Chang and Song (2009) observed a large difference between estimates of the MCD45A1 (MODIS Collection 5 product) and L3JRC burned area products over the period 2000 to 2007 for northern latitudes and found that, over the years, the greatest difference occurred for 2003 and, in general, MDC45A1 estimates were more comparable with GFED2 than to L3JRC.

Emissions from African vegetation fires represent more than one third of the total CO according to ATSR and GFED2 and almost half of it according to MODIS and MOPITT inventories. Africa remains a key continent for the global carbon cycle although it accounts for 14% of the global population and only 3% of the global emissions from fossil fuel use (Williams et al., 2007) that increases if regional specificities (biofuel, two wheel emissions . . .) are taken into account (Assamoi and Liousse, 2010). In this continent in fact emissions due to biomass burning and land use change are comparable to emissions from fossil fuel use and are not negligible in the total balance (Canadell et al., 2009; Williams et al., 2007). In general, vegetation fires from Southern Africa most contribute to the total continental budget of emitted CO with between 51% (GFED2) and 63% (VGT). Only for the MODIS inventory burning in the Northern Hemisphere of the continent produces a greater proportion of emissions (52%) with respect to the south (48%). The proportions between north and south are generally the opposite when the area burned, rather than the emissions, is analysed because of the extensive and frequent fires which occur in the Sudania and Guineo-Congolia/Sudania eco-regions; however, the land cover classes affected by fires in the south, more specifically in the Zambezian eco-region, are characterized by greater fuel loads. When considering the emissions [Tg CO] for the northern part of the continent, we observe the following decreasing ranking: MODIS (191.2), MOPITT (126.4), VGT (112.55), ATSR (89.1) and GFED2 (80.3). For the southern part, the ranking is quite different: VGT (190.3), MODIS (176.4), MOPITT (148.9), ATSR (112.6) and GFED2 (82.3). Despite the calibration applied for correcting the underestimation by the L3JRC burned area product

ACPD
10, 17657–17697, 2010

for GLC2000 classes 3 (open deciduous broadleaved tree cover) and 12 (deciduous closed-open shrubs), lower emissions from VGT are found in those classes over West Africa as observed also by Tansey et al. (2008). GFED2 is confirmed to be the lowest estimate among all (Liousse et al., 2010).

In Oceania MODIS provides the highest estimates (92.6 Tg CO) followed by VGT (74.0 Tg CO) and ATSR, GFED and MOPITT with totals around 60 Tg CO. These values strengthen the hypothesis that the L3JRC burned area product underestimates burning in low and sparse vegetation covers of semi-arid Australia as suggested by previous studies (Chang and Song, 2009). The contribution of Oceania to the global emissions of CO is not negligible (10–15%) and it can be even more important in terms of burned area for its frequent and extensive fires in tropical savannas (Chang and Song, 2009).

Only the VGT inventory identifies boreal fires in Northern Asia as the most important source of CO (39%) with the African contribution ranked second (21%). Large differences between VGT and the other inventories are observed for Europe which contributes as much as 6% to the total annual emissions whereas a negligible contribution from the same continent is estimated by the other inventories (1–2%).

Figure 1 depicts the global patterns of CO sources as derived from the five inventories. Visually, the two extreme pictures are given by VGT with the greatest emissions at the northern latitudes and ATSR with a sparser distribution of CO sources over the globe. MOPITT and GFED2 are characterized by extensive areas of low emissions (yellow cells); in particular, in GFED2, a greater number of sources are identified in Europe, China, North America and Australia, with respect to, for example ATSR, although these areas don't contribute much to the CO totals since GFED2 remains the lowest (Table 2). It must be noted that the spatial patterns of the MOPITT map, which seems to identify emission sources all over the globe, are mainly due to the original grid resolution of the product (i.e. 2.1×2.85°) which was resampled to the common resolution of 0.5×0.5°. Similar effects of resampling are visible also in GFED2. Common patterns of intense burning can be observed, in particular, in the savannas of South America,

ACPD
10, 17657–17697, 2010

Africa and Australia, in the Far East of Russia south of Lake Baikal and along the border with Mongolia and China and in the forested regions of South-East Asia. Only the VGT inventory highlights extensive burning at the northernmost latitudes (above 60° N) of North America and Asia with a consequent contribution of these regions to the global amount of CO emitted due to the high fuel loads. Note that the VGT spatial distribution of CO sources in South America is different compared to the other inventories and emissions are located in the Argentinean savannas rather than in the savannas south of the border with the Amazonian forest.

The difference of spatial patterns of CO emissions is quantified by the correlation analysis which compares two inventories at a time (Table 3). The coefficient of determination (R^2) computed between VGT and each of the other inventories is generally the lowest for the northern continents and it is null for South America due to the different location of CO sources discussed above. In Northern Asia, South America, and Africa the greatest correlation is achieved between MODIS and GFED2 (R^2>0.45); indeed they use the same remotely sensed source for active fires. In North America and Europe the highest R^2 (>0.40) is between ATSR and MODIS while it is between VGT and MODIS (R^2=0.43) in Oceania. In Africa all products show very similar geographical distribution of emissions. Note that a greater value of R^2 means a high spatial correlation of the annual totals between two inventories but not necessarily a good agreement in terms of absolute values. This is the case of South America where identical annual totals for VGT and MOPITT (Table 2) are given by different spatial distributions of CO sources. However, significant regression relationships can be used for inter-calibration of the products. If MOPITT is considered to be an independent estimate of CO emissions, the most similar geographical distribution is given by GFED2 in North America, Northern Asia, and Africa.

At the global level, the agreement is very low and the maximum R^2 is achieved between MODIS and GFED2 (R^2=0.33). The MOPITT inventory is best correlated to MODIS and GFED2; in fact these three products have in common to be largely based on the active fire maps derived from the MODIS sensor; the geographical agreement

ACPD
10, 17657–17697, 2010

was therefore expected.

3.2 Seasonality of CO emissions

Seasonality, i.e. the temporal distribution of monthly emissions, is an important input parameter for both biomass burning studies and models of the circulation of atmospheric pollutants (Kopacz et al., 2010); especially in the case of chemical compounds such as CO which is characterized by a lifetime in the atmosphere of about two months (Crutzen and Zimmermann, 1991).

Figure 2 shows monthly emission estimates given by the five inventories for the continental windows. In North America fire CO emissions start in March/April and lasts, through summer, until October/November; the season peak occurs in August with an amount of emitted CO which varies largely: 19.1, 4.8, 9.0 and 11.3 Tg CO according to ATSR, MODIS, GFED2, and MOPITT, respectively. Instead, VGT shows emissions throughout the year with peaks in May (73.9 Tg CO) and October (32.6 Tg CO). In Europe, emissions are observed from the ATSR, MODIS, GFED2 and MOPITT inventories from March to October with a first peak in spring (April) and a second one in summer (August); absolute values of emissions are low with summer maxima below 3 Tg CO. Also VGT identifies spring emissions although somewhat overestimated (22.7 Tg CO) plus an unlikely fire activity at the end of the year (November and December) which is not detected by the other inventories; in these two months 67% and 73% of the emitted CO comes from fires in closed deciduous broadleaved forests (GLC2000 class 2). In Northern Asia emissions last from March to October. MODIS has a peak of significant entity in May (121.3 Tg CO), which was also observed by other studies relying on ground measurements and satellite observations (Edwards et al., 2004; Yurganov et al., 2005; van der Werf et al., 2006). VGT is characterized by the same early peak in May and a second maximum in September/October when the other inventories detect low emissions. ATSR and MOPITT show high emissions also in July (44.0 and 20.4 Tg CO, respectively). In both Europe and Northern Asia, VGT emissions are of one magnitude greater compared to the other inventories, with 22.7 and

ACPD
10, 17657–17697, 2010

12.3 Tg CO in April and November in Europe and 129.8 and 113.4 Tg CO in May and October in Northern Asia. It is accepted that the L3JRC product overestimates burned areas and therefore emissions at the northernmost latitudes especially outside the fire season (Chang and Song, 2009). In particular, the effect of spring melting of snow and of autumn senescence of vegetation (yellowing and falling leaves) on the spectral signal may have led to mistakenly mapped burned areas. The fact that CO sources in the VGT inventory for Northern Asia in September and October are all located in the GLC2000 class 5 (needle leaves deciduous tree cover) reinforces this hypothesis. However, field data would be necessary to confirm it. The validation exercise carried out by Tansey et al. (2008) does not provide accuracy outside the fire season and the authors themselves suggest a careful use of this data in off-season time.

In the southern windows, the seasonal distribution of monthly emissions is much more similar among the inventories. The best agreement is reached for Africa: the greatest emissions during the Northern and Southern burning seasons appear clearly from the graphs in December/January and July/August, respectively, for all inventories. However, VGT provides the greatest estimates in July (66.1 Tg CO) due to fires mapped in southern savannas whereas the other inventories have the greatest monthly emissions in December and January due to fires in the northern savanna belt. In these two months, the MODIS inventory, for example, has significant emissions from fires in the broadleaved evergreen forest and in mixed savanna/crop areas (GLC2000 classes 1 and 18) (see also Fig. 5). Among all, GFED2 shows the lowest estimates. In South-America, emissions are significant from March to September/October; all inventories agree with this trend, except VGT which appears to identify emissions from fires throughout the year with burning also in January and February with emissions comparable to those released during the summer months. In particular, 50% and 68% of emissions in January and February, respectively, are due to fires in the evergreen needle-leaved forests (GLC2000 class 4). In this continent the lowest emissions are given by MODIS with monthly estimates always below 5 Tg of CO. Finally, in Oceania VGT seasonality is quite different from the other inventories and, like in South

ACPD
10, 17657–17697, 2010

America, it depicts emissions from fires throughout the year with a minimum in December/January. On the contrary, MODIS shows a peak in January (21.25 Tg CO) due to much more extensive burning (72%) in forested areas (GLC2000 class1: evergreen broadleaved forest).

The greatest discrepancies are observed in the seasonal patterns of CO emissions given by VGT for the northern windows. The other inventories provide much more similar seasonality. However, in the southern continental windows the apparent continuous burning throughout the year is a consequence of the fact that these windows contain the equatorial line that further splits them into northern and southern areas with different alternate dry and wet seasons and therefore different timing of burning. A narrower season for the emissions can instead be observed during summer in the northern windows. Note that CO seasonality may be decoupled from seasonality of burned areas due to fires occurring in different land cover classes with different fuel loads and composition (van der Werf et al., 2006). We did not observe any systematic delay of maxima (month of occurrence of the season peak) between *bottom-up* models and the MOPITT dataset; delay which, on the contrary, was pointed out by previous studies (van der Werf et al., 2006; Petron et al., 2004; Arellano et al., 2006).

The results discussed in this section confirm finding by Generoso et al. (2003) who pointed out that global estimates within large regions can be corrected whereas the exact spatial and temporal description can be improved. In fact our analyses highlight the compensation effects hiding behind synthetic totals of emissions. Also Michel et al. (2005) compared emissions from different sources of remote sensing burned area products over Asia and found a higher difference in terms of seasonality than in terms of total quantities.

Figure 3 shows the spatial distribution of the difference between MOPITT (assumed here as the term of comparison) and the other inventories as observed through the regression analysis of the cell monthly CO emissions. Figure 4 depicts the spatial distribution of the proportion of each 0.5×0.5° cell covered by the three broad land cover types derived by grouping together the GLC2000 classes (dark shades highlight

ACPD
10, 17657–17697, 2010

cells dominated by each land cover whereas the lighter colors highlight mixed cells). The distribution of the major land cover types can help in interpreting the results of the correlation analysis. In Fig. 3 a significant portion of the 0.5×0.5° cells shows no correlation (light grey) for seasonality between each inventory compared to MOPITT with as much as 60% of the cells in the case of VGT. However, these figures might be biased by the fact that the MOPITT inventory is derived at a coarser spatial resolution. The number of cells with negative correlation is greater than zero only in the case of VGT and mainly located in the neighbourhood of low correlation regions. The difference between the inventories appear biased towards either a significant underestimation or overestimation: red/magenta and cyan/blue clusters dominate with respect to the green/yellow colors, which represent the lowest difference between the inventories with a slope of the regression line closer to the 1:1 line ($30^\circ < \alpha < 60^\circ$).

In the Northern Hemisphere, VGT is systematically higher than MOPITT and, in particular for agricultural regions of Canada, the US, Eastern Europe and China, and for forest regions of the Russian Federation (red/magenta colors in Fig. 3a). An exception is the cluster of low difference (cyan to yellow colors) in northern Kazakhstan where the land cover is dominated by agriculture and savannas.

South America shows up as a region where VGT underestimates in the mixed savanna and agriculture regions of Brazil and northern Argentina (blue/cyan areas) whereas no correlation is observed for the pampas in Southern Argentina where only VGT identifies CO sources from savanna fires: this issue has already been discussed above and identified as a clear discrepancy between VGT and the other inventories for this continent.

In Africa the difference between VGT and MOPITT has a clear latitudinal range, in both north and south directions, from high overestimation in forested areas of central Africa (red cells) to a small difference in the denser savannas and grasslands (yellow/green) and to a higher underestimation in the drier sub-Saharan savannas and in the Southern Miombo woodlands (blue colors). A very similar pattern can be observed for MODIS (Fig. 3c) in Africa. MODIS shows some clear clusters of underestimation

ACPD
10, 17657–17697, 2010

(blue/cyan) in agricultural regions of Canada, the US and Mexico whereas it is higher than MOPITT (red cells) in agriculture-dominated areas of Eastern Europe and Russia and in forested regions of Russia along the border with Mongolia. This forest region, which is also identified and overestimated by ATSR and GFED2, was in fact severely affected by fires in 2003 as a consequence of exceptional weather anomalies which increase the likelihood of fire ignition and propagation: in this region more than 87% of fires are started by people (Mollicone et al., 2006). Red/magenta clusters are also evident in forests of China and India.

Figure 3d shows that GFED2 underestimates MOPITT in all regions of the globe with some small exceptions in Canada, Northern Europe and Russia, central Siberia, Venezuela and Brazil and central Africa. The dominant blue/cyan clusters confirm that the lower estimates of CO emissions from GFED2, which provides the lowest total emissions (Table 2), are uniformly distributed with no spatial bias over the globe.

The MODIS-MOPITT comparison shows underestimation in South America, like GFED2, and a spatial distribution of the difference in Africa more similar to VGT.

Finally, the patterns of MOPITT-ATSR correlation highlights the lower CO emission sources identified by nighttime active fires especially in agricultural areas of Europe, North America and China: other authors have in fact pointed out that ATSR WFA has a relatively low detection rate of agricultural fires which mainly burn during daytime (Le Page et al., 2008).

3.3 CO emissions per land cover

Table 4 summarizes the proportion of the three broad land covers within the continental windows: on average savanna/grasslands occupy 41% of the land Earth surface, whereas forest and agriculture cover 36 and 23%, respectively. Note that these percentages are computed by taking into account only fire prone land cover types; yet the remaining classes cover a small proportion of the land surface. Table 5 reports emissions as Teragrams of CO and as percentage given by VGT, ATSR, and MODIS inventories for forest, savanna/grasslands and agriculture biomes; for the globe the

ACPD
10, 17657–17697, 2010

percentage of burned area responsible for the emission is also shown.

More than 70% of the global CO emissions from vegetation fires in 2003 came from forests as estimated from the VGT and MODIS inventories and 64% according to ATSR whilst the area burned accounted only for between 19–27%. Note that, similar proportional contributions over the globe may hide a large difference in terms of the amount of emitted CO, such as in the case of agriculture (3–4%; 22.2–43.4 Tg CO). In the forest biome, VGT provides the greatest estimates for all continents except Africa and Oceania where MODIS estimates are the greatest due to the anomalous contribution in December–February (ten times greater than VGT and ATSR) of the evergreen broadleaved forest (GLC2000 class 1) as also observed in Fig. 2. Significant contributors to global CO budget are fires in the boreal forests of the Russian Federation (22–35%). ATSR shows that 12% of the global emissions are due to fires in South American forests whereas MODIS shows a similar contribution of forests in Oceania. These remarks confirm findings by Michel et al. (2005) who highlighted that the interannual difference in total amounts of CO emissions in Asia from different remotely sensed burned area products were often given by the forest classes which, with high biomass densities, greatly contribute to the total emissions. Moreover, forests more than other land covers play a key role in the global budget of reduced chemical species, such as CO, which are the product of the incomplete combustion of live biomass (see also emissions factors in Mieville et al., 2010). Despite an increase in the accuracy of burned area maps, an accurate parameterization of vegetation characteristics and conditions at the time of fire occurrence is highly recommended.

Although between 53% and 63% of the total burned area is in savannas and grasslands, their contribution to CO emissions is in the range 23–32%; between 13% and 19% of these emissions are from fires in Africa which are identified as the most important source of emissions in the savanna biome from all of the three inventories. The range of estimates of total emissions from savannas and grasslands is 173.0–324.3 Tg CO with ATSR and MODIS almost identical despite a different distribution among the continents. The largest difference is seen for South American savannas where MODIS

ACPD
10, 17657–17697, 2010

estimates are of one order of magnitude lower than the other two inventories.

Finally, agricultural fires which account for about 20% of the total burned area, are responsible of only 3–4% of the global CO emissions. Although they little contribute compared to the other two biomes globally, they might become significant at the continental scale. For example, in Europe the contribution of agriculture fires is in the range 8–10%. For these fires, a major issue is that the majority of the burned areas are small compared to the sensor's pixel size and may therefore be undetected. Our analyses show that, only in agricultural areas of Oceania, ATSR and MODIS estimates are systematically greater than VGT and the highest estimate is given by MODIS in Africa (20.3 Tg CO).

The seasonality of CO emissions per land cover type is shown in Fig. 5. First of all, it highlights the high values from VGT over the northern windows and outside the typical fire season (April/May to August/September) when, as observed by Chang and Song (2009), the L3JRC product is less reliable. In the forest land cover of Africa, MODIS clearly overestimates emissions in January thus leading to the anomaly already highlighted in Fig. 2. In African savanna/grasslands VGT is the only inventory which clearly identifies the two peaks of the northern and southern fire seasons; the other two inventories underestimates emissions between June and August due to fires in southern savannas. In South American savannas the three inventories have significantly different seasonality. In agriculture regions of the northern windows CO emissions have two peaks although VGT overestimates; the most similar trend between the inventories can be observed for Northern Asia with intense emissions in May and October due to fires in permanent agriculture regions of Russia, Ukraine and Kazakhstan also shown in Fig. 4: here fires before planting and after harvest are a quite common land management (Korontzi et al., 2006). In Europe, where agriculture fires are important, the three inventories provide a different seasonality and only VGT well highlights the two peaks typical of managed areas (spring and autumn).

In South-America ATSR estimates are greater than the others and show peaks in March and September: the detailed classes contributing to these two maxima are

ACPD
10, 17657–17697, 2010

the shrub/grass and crop mosaic (GLC2000 class 18) and cultivated/managed areas (GLC2000 class 16), respectively, with almost 0.7 Tg CO each. Two noticeable cases are agriculture fires in Africa where MODIS emissions, mainly concentrated between November and January, are significantly greater (with a total of 20.3 Tg CO) and in Oceania where MODIS and ATSR show the same total amount (about 2.0 Tg CO) and the same seasonality. In the first case, despite the difference in the total amount of CO, monthly maps show very similar geographical distribution of emission sources, located in the northern sub-Saharan belt with residual burning in South-East Africa; this difference is a consequence of the discrepancies in the amount of area burned as used by the three inventories. The same occurs in Australia (data not shown): similar spatial patterns of CO sources but different intensity due to the difference in the rate of area burned as derived from the remotely sensed products.

4 Conclusions

The objective of this work was to compare five inventories of global CO emissions from vegetation fires derived from satellite data for the year 2003. We named the inventories VGT, ATSR, MODIS, GFED2 and MOPITT after the name of the sensor used to derive fire information. The strength of our work is the number of inventories taken into account and the fact that different data and models have been compared: *bottom-up* and *top-down* approaches, active fire counts and burned area maps derived from different satellite sensors, common fixed broad land cover type and fuel loads based on biogeochemical model, fixed and time dependent burning efficiency. Despite the improvement brought by the recent and newer satellite based burned area products, large uncertainty still remains in the estimation of emissions which globally range between 398 Tg CO (GFED2) and 1422 Tg CO (VGT). The greatest difference is observed for the northern regions of the globe and, in particular, for Eurasian forests where VGT significantly overestimates emissions outside the fire season. In 2003 forest fires contributed 64–74% to the global CO emissions despite accounting for *only* 19–27% of

ACPD
10, 17657–17697, 2010

the total area burned.

The GFED2 inventory gives the lowest values except for South America where MODIS is even lower due to underestimation of emissions mainly from the savanna/grasslands land cover.

The best agreement among the inventories is observed for Africa which is an important contributor with emissions from savanna fires (13–19%). CO emissions from both African savannas and Eurasian boreal forests contribute more than 40% to the global CO budget. In Africa only VGT clearly shows both seasonal peaks due to burning in the northern and Southern Hemispheres and an anomaly was observed in the MODIS inventory which shows exceptionally high emissions from forest and agriculture land covers in December/January. Globally, savannas which account for as much as 53–63% of the global burned area contributed with 23–32% to the total CO emissions.

In South America important differences are given by the low emissions from MODIS in savanna/grasslands compared to the other inventories and the significantly different geographical distribution of CO sources provided by the VGT inventory with emissions mainly from savannas in Argentina rather than in Brazil.

If the MOPITT inventory is assumed as an independent estimate, the combined analysis of the geographical distribution and the seasonality of CO sources as given by the VGT, ATSR, MODIS and GFED2 inventories, confirms the large difference biased towards the general overestimation from VGT and underestimation from GFED2. These results confirm that estimates are more comparable when annual and/or regional totals are computed thus strengthening findings by previous studies (Michel et al., 2005).

We found no evidence that products derived from active fire counts globally better or worse depict burning activity compared to burned area. The idea of complementarity between the information brought by hot spots and burned areas is not new in the fire remote sensing community. However, to our knowledge, nobody has actually proposed a global methodology to integrate the two fire products and benefit from their respective advantages. Moreover, a third type of fire product derived from EO (Earth Observation) systems is becoming available: the Fire Radiative Power (FRP, Wooster et al., 2005),

ACPD
10, 17657–17697, 2010

measured over active fires, provided by the MODIS sensor and by the SEVIRI (Spinning Enhanced Visible and InfraRed Imager) sensor onboard the Meteosat Second Generation (MSG) platform. This relatively new fire product offers the advantage to be directly linked to the intensity of the fire and therefore to both the quantity of fuel which is burned and to the burning conditions. FRP is therefore a very good candidate for any assessment of emissions from fires although it relies on active fires observed by the EO systems which are a temporal sampling of the burning activity. Since validation of datasets of CO emissions at the global scale is not feasible, there is a clear need of improving not only the accuracy of remotely sensed burned area products but also the characterization of vegetation types and conditions (fuel loads, burning efficiency and emission factors) especially over forests which so greatly contribute to the CO budget. Above all, a geographical distribution of fuel loads more detailed than the broad land cover classes given by global maps such as the GLC2000 and a time-dependent characterization of fuel conditions should be addressed in the future.

Acknowledgements. The authors would like to acknowledge D. Simonetti for post-processing the L3JRC global product over Africa and C. Zambrano for the processing of CO inventories in the preliminary phases of the project. This work has been done in the frame of ACCENT European network (http://www.accent-network.org) together with the GEIA (Global Emissions Inventory Activity of IGBP).

References

Andreae, M. O. and Merlet, P.: Emission of trace gases and aerosols from biomass burning, Global Biogeochem. Cy., 15, 955–966, 2001.

Anyamba, A., Justice, C. O., Tucker, C. J., and Mahoney, R.: Seasonal to interannual variability of vegetation and fires at SAFARI 2000 sites inferred from advanced very high resolution radiometer time series data, J. Geophys. Res., 108(D13), 8507, doi:10.1029/2002JD002464, 2003.

Arellano, A. F., Kasibhatla, P. S., Giglio, L., van der Werf, G. R., Randerson, J. T., and Collatz, G. J.: Time-dependent inversion estimates of global biomass-burning CO emissions

ACPD

10, 17657–17697, 2010

using Measurement of Pollution in the Troposphere (MOPITT) measurements, J. Geophys. Res., 111, D09303, doi:10.1029/2005JD006613, 2006.
Arino, O. and Plummer, S.: The Along Track Scanning Radiometer World Fire Atlas – Detection of night-time fire activity, IGBP-DIS Working Paper #23. Postdam, Germany, 2001.
Assamoi, E. and Liousse, C.: Focus on the impact of two wheel vehicles on African combustion aerosols emissions, Atmos. Environ., in review, 2010.
Barbosa, P. M., Stroppiana, D., Grégoire, J.-M., and Pereira, J. C. M.: An assessment of vegetation fire in Africa (1981–1991): burned area, burned biomass, and atmospheric emissions, Global Biogeochem. Cy., 13(4), 933–950, 1999.
Bartholomé, E. and Belward, A.: GLC2000: a new approach to global land cover mapping from Earth observation data, Int. J. Remote Sens., 26(9), 1959–1977, 2005.
Bergamaschi, P., Hein, R., Heimann, M., and Crutzen, P. J.: Inversion modeling of the global CO cycle: 1. Inversion of CO mixing ratios, J. Geophys. Res., 105(D2), 1909–1927, 2000.
Boschetti, L., Eva, H. D., Brivio, P. A., and Grégoire, J.-M.: Lessons to be learned from the comparison of three satellite-derived biomass burning products, Geophys. Res. Lett., 31(21), L21501, 1–4, 2004.
Canadell, J. G., Raupach, M. R., and Houghton, R. A.: Anthropogenic CO_2 emissions in Africa, Biogeosciences, 6, 463–468, doi:10.5194/bg-6-463-2009, 2009.
Chang, D. and Song, Y.: Comparison of L3JRC and MODIS global burned area products from 2000 and 2007, J. Geophys. Res., 114, D16106, doi:10.1029/2008JD011361, 2009.
Chevallier, F., Fortems, A., Bousquet, P., Pison, I., Szopa, S., Devaux, M., and Hauglustaine, D. A.: African CO emissions between years 2000 and 2006 as estimated from MOPITT observations, Biogeosciences, 6, 103–111, doi:10.5194/bg-6-103-2009, 2009.
Chin, M., Ginoux, P., Kinne, S., Torres, O., Holben, B. N., Duncan, B. N., Martin, R. V., Logan, J. A., Higurashi, A., and Nakajima, T.: Tropospheric aerosol optical thickness from the GOCART Model and comparisons with satellite and sun photometer measurements, J. Atmos. Sci., 59, 461–483, 2002.
Conard, S. G., Sukhinin, A. I., Stocks, B. J., Cahoon, D. R., Davidenko, E. P., and Ivanova, G. A.: Determining effects of area burned and fire severity on carbon cycling and emissions in Siberia, Climatic Change, 55, 197–211, 2002.
Cooke, W. F., Koffi, B., and Grégoire, J. M.: Seasonality of vegetation fires in Africa from remote sensing data and application to a global chemistry model, J. Geophys. Res., 101, 21051–21065, 1996.

ACPD
10, 17657–17697, 2010

Crutzen, P. J., Heidt, L. E., Krasnec, J. P., Pollock, W. H., and Seiler, W.: Biomass burning as a source of atmospheric gases CO, H_2, N_2O, NO, CH_3CL and COS, Nature, 282, 253–256, 1979.

Crutzen, P. J. and Zimmermann, P. H.: The changing photochemistry of the troposphere, Tellus, 43AB, 136–151, 1991.

Dwyer, E., Pinnock, S., Grégoire, J.-M., and Pereira, J. M. C.: Global spatial and temporal distribution of vegetation fires as determined from satellite observations, Int. J. Remote Sens., 21, 1289–1302, 2000.

Edwards, D. P , Emmons, L. K., Hauglustaine, D. A., Chu, A., Gille, J. C., Kaufman, Y. J., Petron, G., Yurganov, L. N., Giglio, L., Deeter, M. N., Yudin, V., Ziskin, D. C., Warner, J., Lamarque, J.-F., Francis, G. L., Ho, S. P., Mao, D., Chen, J., Grechko, E. I., and Drummond, J. R.: Observations of carbon monoxide and aerosols from the Terra satellite: Northern Hemisphere variability, J. Geophys. Res., 109, D24202, doi:10.1029/2004JD004727, 2004.

Friedli, H. R., Arellano, A. F., Cinnirella, S., and Pirrone, N.: Initial estimates of mercury emissions to the atmosphere from global biomass burning, Environ. Sci. Technol., 43, 3507–3513, 2009.

Generoso, S., Bréon, F.-M., Balkanski, Y., Boucher, O., and Schulz, M.: Improving the seasonal cycle and interannual variations of biomass burning aerosol sources, Atmos. Chem. Phys., 3, 1211–1222, doi:10.5194/acp-3-1211-2003, 2003.

Giglio, L., van der Werf, G. R., Randerson, J. T., Collatz, G. J., and Kasibhatla, P.: Global estimation of burned area using MODIS active fire observations, Atmos. Chem. Phys., 6, 957–974, doi:10.5194/acp-6-957-2006, 2006.

Grégoire, J.-M., Tansey, K., and Silva, J. M. N.: The GBA2000 initiative: developing a global burned area database from SPOT-VEGETATION imagery, Int. J. Remote Sens., 24(6), 1369–1376, 2003.

Hély, C., Dowty, P. R., Alleaume, S., Caylor, K. K., Korontzi, S., Swap, R. J., Shugart, H. H., and Justice, C. O.: Regional fuel load for two climatically contrasting years in Southern Africa, J. Geophys. Res., 108(D13), 8475, doi:10.1029/2002JD002341, 2003.

Hobbs, P. V., Reid, J. S., Kotchenruther, R. A., Ferek, R. J., and Weiss, R.: Direct radiative forcing by smoke from biomass burning, Science, 275, 1776–1778, 1997.

Horowitz, L. W., Walters S., Mauzerall, D. L., et al.: A global simulation of tropospheric ozone and related tracers: description and evaluation of MOZART, version 2, J. Geophys. Res.,

ACPD

10, 17657–17697, 2010

108, 4784, doi:10.1029/2002JD002853, 2003.
Innes, J. L., Beniston, M., and Verstraete, M. M. (Eds.): Biomass burning & its inter-relations with the climate system, Kluwer Academic Publishers, The Netherlands, 2000.
IPCC-Intergovernmental Panel on Climate Change 2001, Climate Change 2001, The scientific basis, available online at: http://www.ipcc.ch/ipccreports/tar/wg1/index.htm (last access: 30 June 2010), 2001.
IPCC-Intergovernmental Panel on Climate Change 2007, Climate Change 2007, The physical science basis, available online at: http://www.ipcc.ch/ipccreports/ar4-wg1.htm (last access: 30 June 2010), 2007.
Jain, A. K.: Global estimation of CO emissions using three sets of satellite data for burned area, Atmos. Environ., 41, 6931–6940, 2007.
Justice, C. O., Giglio, L., Korontzi, S., Owens, J., Morisette, J., Roy, D., Descloitres, J., Alleaume, S., Petitcolin, F., and Kaufman, T.: The MODIS fire products, Remote Sens. Environ., 83, 244–262, 2002.
Konare, A., Liousse, C., Guillaume, B., Solmon, F., Assamoi, P., Rosset, R., Gregoire, J. M., and Giorgi, F.: Combustion particulate emissions in Africa: regional climate modeling and validation, Atmos. Chem. Phys. Discuss., 8, 6653–6681, doi:10.5194/acpd-8-6653-2008, 2008.
Kopacz, M., Jacob, D. J., Fisher, J. A., Logan, J. A., Zhang, L., Megretskaia, I. A., Yantosca, R. M., Singh, K., Henze, D. K., Burrows, J. P., Buchwitz, M., Khlystova, I., McMillan, W. W., Gille, J. C., Edwards, D. P., Eldering, A., Thouret, V., and Nedelec, P.: Global estimates of CO sources with high resolution by adjoint inversion of multiple satellite datasets (MOPITT, AIRS, SCIAMACHY, TES), Atmos. Chem. Phys., 10, 855–876, doi:10.5194/acp-10-855-2010, 2010.
Korontzi, S., McCarty, J., Loboda, T., Kumar, S. and Justice, C.: Global distribution of agricultural fires in croplands from 3 yr of Moderate Resolution Imaging Spectroradiometer (MODIS) data, Global Biogeochem. Cy., 20, G2021, doi:10.1029/2005GB002529, 2006.
Langenfelds, R. L., Francey, R. J., Pak, B. C., Steele, L. P., Lloyd, J., Trudinger, C. M., and Allison, C. E.: Interannual growth rate variations of atmospheric CO_2 and its $\delta^{13}C$, H_2, CH_4 and CO between 1992 and 1999 linked to biomass burning, Global Biogeochem. Cy., 16(3), 1048, doi:10.1029/2001GB001466, 2002.
Langmann, B., Duncan, B., Textor, C., Trentmann, J., and van der Werf, G. R.: Vegetation fire emissions and their impact on air pollution and climate, Atmos. Environ., 43, 107–116, 2009.
Le Page, Y., Pereira, J. M. C., Trigo, R., da Camara, C., Oom, D., and Mota, B.: Global fire

ACPD
10, 17657–17697, 2010

activity patterns (1996–2006) and climatic influence: an analysis using the World Fire Atlas, Atmos. Chem. Phys., 8, 1911–1924, doi:10.5194/acp-8-1911-2008, 2008.
Liousse, C., Penner J. E., Walton J. J., Eddleman H., Chuang C., and Cachier H.: Modelling biomass burning aerosols, in: Biomass Burning and Global Change, edited by: Levine J. S., MIT Press, Cambridge, 492–508, 1996.
Liousse, C., Andreae, M. O., Artaxo, P., Barbosa, P., Cachier, H., Grégoire, J. M. , Hobbs, P., Lavoué, D., Mouillot, F., Penner, J., and Scholes, M.: Deriving global quantitative estimates for spatial and temporal distributions of biomass burning emissions, in: Emissions of Atmospheric Trace Compounds, edited by: Granier, C., Artaxo, P., and Reeves, C., Kluwer Academic Publishers, Dordrecht, The Netherlands, 544 pp., 2004.
Liousse, C., Guillaume, B., Grégoire, J. M., Mallet, M., Galy, C., Pont, V., Akpo, A., Bedou, M., Castéra, P., Dungall, L., Gardrat, E., Granier, C., Konaré, A., Malavelle, F., Mariscal, A., Mieville, A., Rosset, R., Serça, D., Solmon, F., Tummon, F., Assamoi, E., Yoboué, V., and Van Velthoven, P.: Western african aerosols modelling with updated biomass burning emission inventories in the frame of the AMMA-IDAF program, Atmos. Chem. Phys. Discuss., 10, 7347–7382, doi:10.5194/acpd-10-7347-2010, 2010.
Liu, J., Drummond, J. R., Li, Q., Gille, J. C., and Ziskin, D. C.: Satellite mapping of CO emission from forest fires in Northwest America using MOPITT measurements, Remote Sens. Environ., 95, 502–516, 2005.
Manning, M. R., Brenninkmeijer, C. A. M., and Allan, W.: The atmospheric carbon monoxide budget of the Southern Hemisphere: implication of $^{13}C/^{12}C$ measurements, J. Geophys. Res., 102, 10673–10682, 1997.
Mieville, A., Granier, C., Liousse, C., Guillaume, B., Mouillot, F., Lamarque, J.-F., Grégoire, J.-M., and Pétron, G.: Emissions of gases and particles from biomass burning during the 20th century using satellite data and an historical reconstruction, Atmos. Environ., 44, 1469–1477, 2010.
Michel, C., Liousse, C., Grégoire, J.-M., Tansey, K., Carmichael, G. R., and Woo, J.-H.: Biomass burning emission inventory from burn area data given by the SPOT-VEGETATION system in the fram of TRACE-P and ACE-Asia campaigns, J. Geophys. Res., 110, D09304, doi:10.1029/2004JD005461, 2005.
Mollicone, D., Eva, H., and Achard, F.: Human role in Russian wild fires, Nature, 440, 436–437, 2006.
Mota, B. W., Pereira, J. M. C., Oom, D., Vasconcelos, M. J. P., and Schultz, M.: Screen-

ACPD
10, 17657–17697, 2010

ing the ESA ATSR-2 World Fire Atlas (1997–2002), Atmos. Chem. Phys., 6, 1409–1424, doi:10.5194/acp-6-1409-2006, 2006.

NASA/University of Maryland: MODIS Hotspot/Active Fire Detections. Data set. MODIS Rapid Response Project, NASA/GSFC [producer], University of Maryland, Fire Information for Resource Management System [distributors], http://maps.geog.umd.edu/firms/firedata.htm (last access: 30 June 2010), 2002.

Novelli, P. C., Masarie, K. A., Lang, P. M., Hall, B. D., Myers, R. C., and Elkins, J. W.: Reanalysis of tropospheric CO trends: effects of the 1997–1998 wildfires, J. Geophys. Res.-Atmos., 108(D15), 4464, doi:10.1029/2002JD003031, 2003.

Pétron, G., Granier, C., Khattatov, B., Yudin, V., Lamarque, J.-F., Emmons, L., Gille, J., and Edwards, D. P.: Monthly CO surface sources inventory based on the 2000–2001 MOPITT satellite data, Geophys. Res. Lett., 31, L21107, doi:10.1029/2004GL020560, 2004.

Pétron, G., Granier, C., Khattatov, B., Larmarque, J.-F., Yudin, V., Muller, J.-F., and Gille, J. : Inverse modeling of carbon monoxide surface emissions using CMDL network observations, J. Geophys. Res., 107(D24), 4762, doi:10.1029/2001JD002049, 2002.

Podgorny, I. A., Li, F., and Rammanathan, V.: Large aerosol radiative forcing due to the 1997 Indonesian forest fire, Geophys. Res. Lett., 30(1), 1028, doi:10.1029/2002GL015979, 2003.

Reid, J. S., Koppmann, R., Eck, T. F., and Eleuterio, D. P.: A review of biomass burning emissions part II: intensive physical properties of biomass burning particles, Atmos. Chem. Phys., 5, 799–825, doi:10.5194/acp-5-799-2005, 2005.

Seiler, W. and Crutzen, P. J.: Estimate of gross and net fluxes of carbon between the biosphere and the atmosphere from biomass burning, Climate Change, 2, 207–247, 1980.

Schultz, M. G.: On the use of ATSR fire count data to estimate the seasonal and interannual variability of vegetation fire emissions, Atmos. Chem. Phys., 2, 387–395, doi:10.5194/acp-2-387-2002, 2002.

Stroppiana, D., Brivio, P. A., and Grégoire, J.-M.: Modelling the impact of vegetation fires, detected from NOAA-AVHRR data, on tropospheric chemistry in tropical Africa, in: Biomass burning & its inter-relations with the climate system, Kluwer Academic Publishers, The Netherlands, 193–213, 2000.

Tansey, K., Grégoire, J. M., Stroppiana, D., Sousa, A., Silva, J., Pereira, J. M. C., Boschetti, L., Maggi, M., Brivio, P. A., Fraser, R., Flasse, S., Ershov, D., Binaghi, E., Graetz, D., and Peduzzi, P.: Vegetation burning in the year 2000: global burned area estimates from SPOT vegetation data, J. Geophys. Res., 109, D14S03, doi:10.1029/2003JD003598, 2004.

ACPD
10, 17657–17697, 2010

Tansey, K., Grégoire, J. M., Defourny, P., Leigh, R., Pekel, J. F., Van Bogaert, E., and Bartholomè, E.: A new, global, multi-annual (2000–2007) burnt area product at 1 km resolution, Geophys. Res. Lett., 35, L01401, doi:10.1029/2007GL031567, 2008.

van der Werf, G. R., Randerson, J. T., Collatz, G. J., Giglio, L., Kasibhatla, P. S., Arellano, A. F., Olsen, S. C., and Kasichke, E.: Continental-scale partitioning of fire emissions during the 1997 to 2001 El Nino/La Nina period, Science, 303, 73–76, 2004.

van der Werf, G. R., Randerson, J. T., Giglio, L., Collatz, G. J., Kasibhatla, P. S., and Arellano Jr., A. F.: Interannual variability in global biomass burning emissions from 1997 to 2004, Atmos. Chem. Phys., 6, 3423–3441, doi:10.5194/acp-6-3423-2006, 2006.

Westerling, A. L., Hidalgo, H. G., Cayan, D. R., and Swetnam, T. W.: Warming and earlier spring increase western US forest wildfire activity, Science, 313, 940–943, doi:10.1126/science.1128834, 2006.

Williams, C. A., Hanan, N. P., Neff, J. C., Scholes, R. J., Berry, J. A., Denning, A. S., and Baker, D. F.: Africa and the global carbon cycle, Carbon Balance Manage., 2(3), doi:10.1186/1750-0680-2-3, 2007.

Wooster, M. J., Roberts, G., Perry, G. L. W., and Kaufman, Y. J.: Retrieval of biomass combustion rates and totals from fire radiative power observations: FRP derivation and calibration relationships between biomass consumption and fire radiative energy release, J. Geophys. Res., 110, D24311, doi:10.1029/2005JD006318, 2005.

Yan, X., Ohara, T., and Akimoto, H.: Bottom-up estimate of biomass burning in mainland China, Atmos. Environ., 40, 5262–5273, 2006.

Yurganov, L. N., Duchatelet, P., Dzhola, A. V., Edwards, D. P., Hase, F., Kramer, I., Mahieu, E., Mellqvist, J., Notholt, J., Novelli, P. C., Rockmann, A., Scheel, H. E., Schneider, M., Schulz, A., Strandberg, A., Sussmann, R., Tanimoto, H., Velazco, V., Drummond, J. R., and Gille, J. C.: Increased Northern Hemispheric carbon monoxide burden in the troposphere in 2002 and 2003 detected from the ground and from space, Atmos. Chem. Phys., 5, 563–573, doi:10.5194/acp-5-563-2005, 2005.

ACPD
10, 17657–17697, 2010

Table 1. Remotely sensed CO emission inventories considered in this analysis for the year 2003.

Inventory	Fire observations	Global product	EO system	Reference
VGT	Burned area	L3JRC 2000-07 [a]	SPOT-VGT	Liousse et al., 2010
ATSR	Nighttime active fires	WFA 2003–2005 [b]	AATSR	Mieville et al., 2010
MODIS	Active fires	MODIS 2001–2004 [c, d]	MODIS	Chin et al., 2002
GFEDv2	Active fires	MODIS 2001–2004 [d]	MODIS	Van der Werf et al., 2006
MOPITT	Active fires	MODIS 2001–2004 [d]	MOPITT	Pétron et al., 2004

[a] Tansey et al., 2008
[b] Arino and Plummer, 2001
[c] Justice et al., 2002
[d] Giglio et al., 2006

ACPD
10, 17657–17697, 2010

Table 2. Total CO emissions for the globe and the continents given in [Tg] and the percentage computed with respect of the global totals. MOPITT values are highlighted in bold as it is the only *top-down* model.

	Total CO [Tg]					Percentage [%]				
	VGT	ATSR	MODIS	GFED2	**MOPITT**	VGT	ATSR	MODIS	GFED2	**MOPITT**
N. America	277.6	48.1	19.2	14.9	**25.5**	19	9	2	4	**4**
Europe	87.8	7.3	13.2	3.5	**9.3**	6	1	2	1	**2**
N. Asia	559.1	139.5	241.6	79.6	**102.0**	39	25	31	20	**17**
S. America	121.7	93.1	35.6	78.1	**121.9**	9	17	5	20	**21**
Africa	302.7	201.7	367.4	162.4	**274.8**	21	37	48	41	**46**
Oceania	74.0	57.9	92.6	59.4	**60.5**	5	11	12	15	**10**
GLOBAL	1422.0	547.5	769.6	397.9	**594.0**	100	100	100	100	**100**

ACPD
10, 17657–17697, 2010

Table 3. The coefficient of determination R^2 derived by regressing CO estimates for the 0.5° cells for each window and the globe. In the parenthesis the number of cells used in the regression after discarding cells with zero emissions in both products. The number of cells for the MOPITT inventory is systematically much higher due to the lower spatial resolution of this product.

		VGT	ATSR	MODIS	GFED2	MOPITT
N. Am.	VGT	1				
	ATSR	0.04 (9067)	1			
	MODIS	0.08 (9254)	0.49 (3217)	1		
	GFED2	0.02 (9818)	0.13 (6920)	0.09 (5999)	1	
	MOPITT	**0.02 (13 040)**	**0.05 (12 376)**	**0.07 (12 371)**	**0.13 (12 378)**	**1**
Europe	VGT	1				
	ATSR	0.08 (5017)	1			
	MODIS	0.21 (5197)	0.40 (3115)	1		
	GFED2	0.08 (5923)	0.15 (5271)	0.18 (4739)	1	
	MOPITT	**0.05 (10 526)**	**0.03 (10 448)**	**0.05 (10 449)**	**0.07 (10 445)**	**1**
N. Asia	VGT	1				
	ATSR	0.08 (14 112)	1			
	MODIS	0.14 (14 579)	0.38 (6650)	1		
	GFED2	0.12 (16 007)	0.30 (12 826)	0.57 (11 303)	1	
	MOPITT	**0.10 (19 579)**	**0.12 (19 331)**	**0.22 (19 320)**	**0.36 (19 343)**	**1**
S. Am.	VGT	1				
	ATSR	0.00 (5309)	1			
	MODIS	0.00 (6410)	0.20 (5497)	1		
	GFED2	0.00 (7773)	0.12 (7446)	0.45 (6906)	1	
	MOPITT	**0.00 (13 636)**	**0.12 (13 625)**	**0.17 (13 627)**	**0.09 (13 165)**	**1**
Africa	VGT	1				
	ATSR	0.27 (5100)	1			
	MODIS	0.44 (5895)	0.37 (5290)	1		
	GFED2	0.44 (7156)	0.29 (6955)	0.63 (6580)	1	
	MOPITT	**0.44 (13 634)**	**0.21 (13 626)**	**0.47 (13 630)**	**0.54 (13 625)**	**1**

ACPD
10, 17657–17697, 2010

Table 3. Continued.

		VGT	ATSR	MODIS	GFED2	MOPITT
Oceania	VGT	1				
	ATSR	0.14 (4401)	1			
	MODIS	0.43 (5567)	0.12 (4613)	1		
	GFED2	0.13 (6722)	0.04 (6520)	0.16 (6088)	1	
	MOPITT	**0.07 (16 257)**	**0.09 (16 257)**	**0.05 (16 257)**	**0.05 (16 257)**	**1**
Global	VGT	1				
	ATSR	0.11 (43 018)	1			
	MODIS	0.20 (46 873)	0.28 (28 255)	1		
	GFED2	0.08 (53 309)	0.15 (45 708)	0.33 (46 210)	1	
	MOPITT	**0.13 (89 275)**	**0.15 (88 195)**	**0.21 (88 169)**	**0.23 (88 234)**	**1**

ACPD
10, 17657–17697, 2010

Table 4. Spatial distribution [10^6 km^2] and proportion [%] of the land area covered by each class for the continental windows and for the globe.

Land cover	N.America		Europe		N. Asia		S.America		Africa		Oceania		Globe	
Forest	7.67	45	3.05	33	10.10	41	8.80	46	4.08	21	3.83	25	**37.53**	**36**
Sav&Grass	7.29	43	2.33	25	9.71	39	5.46	29	11.08	58	7.52	49	**43.37**	**41**
Agriculture	2.05	12	3.87	42	5.02	20	4.70	25	4.05	21	4.15	27	**23.85**	**23**

ACPD
10, 17657–17697, 2010

Table 5. Contribution of forest, savanna/grasslands (SaGra) and agriculture (Agr) to the total annual CO emissions over the continental windows and the globe [Tg/y, %]. In the last column, for the globe we also provide percentage of burned area [BA%] in each class.

Emissions	N.Am. Tg/y, %	Europe Tg/y, %	N. Asia Tg/y, %	S.Am. Tg/y, %	Africa Tg/y, %	Oceania Tg/y, %	Globe Tg/y, %, BA %
Forest VGT	260.3, 18	71.7, 5	499.1, 35	87.0, 6	106.2, 7	30.1, 2	**1054.3, 74, 26**
Forest ASTR	45.4, 8	5.3, 1	122.8, 22	63.9, 12	93.9, 17	20.9, 4	**352.3, 64, 19**
Forest MODIS	18.5, 2	10.5, 1	220.0, 29	31.8, 4	208.8, 27	71.7, 9	**561.2, 73, 27**
SaGra VGT	13.3, 1	4.6, 0	43.7, 3	32.5, 2	187.1, 13	43.1, 3	**324.3, 23, 56**
SaGra ATSR	2.4, 0	0.8, 0	10.5, 2	23.0, 4	101.3, 19	35.0, 6	**173.0, 32, 63**
SaGra MODIS	0.6, 0	1.1, 0	13.4, 2	2.3, 0	138.3, 18	19.0, 2	**174.7, 23, 53**
Agric VGT	3.1, 0	11.5, 1	16.4, 1	2.3, 0	9.4, 1	0.7, 0	**43.4, 3, 18**
Agric ATSR	0.3, 0	1.2, 0	6.2, 1	6.1, 1	6.4, 1	2.0, 0	**22.2, 4, 18**
Agric MODIS	0.1, 0	1.6, 0	7.0, 1	1.5, 0	20.3, 3	1.9, 0	**32.4, 4, 21**

ACPD
10, 17657–17697, 2010

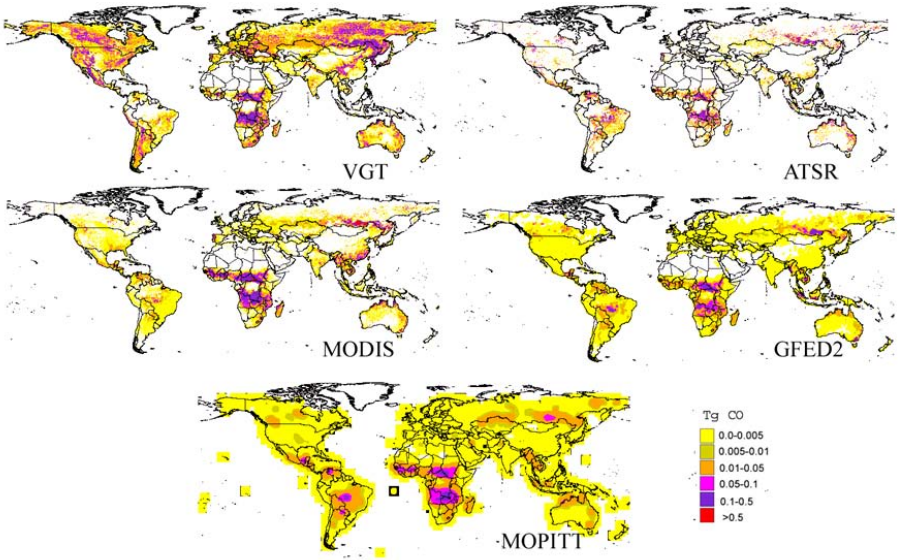

Fig. 1. Maps of total CO emissions [Tg CO] for the year 2003 for 0.5 grid cells.

ACPD
10, 17657–17697, 2010

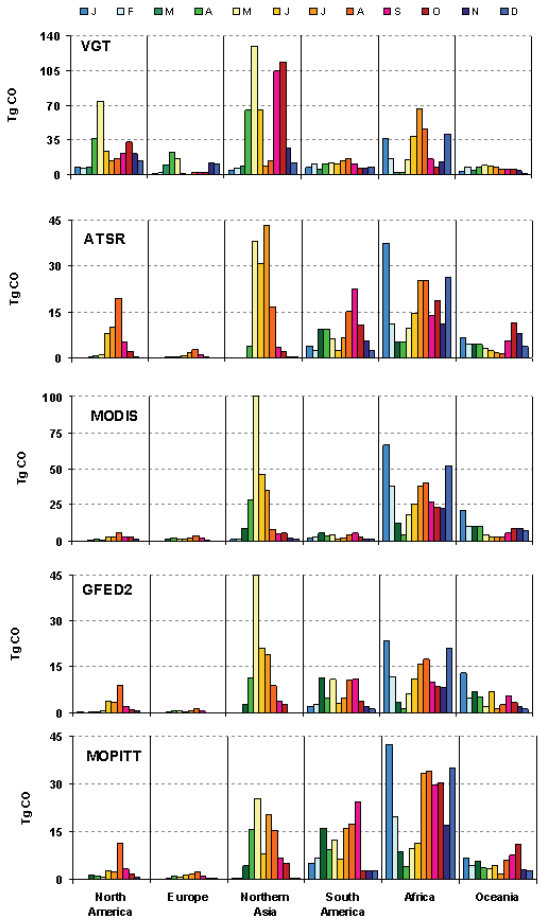

Fig. 2. Seasonality of CO emissions [Tg CO month^{-1}] for the continental windows from the five inventories.

ACPD
10, 17657–17697, 2010

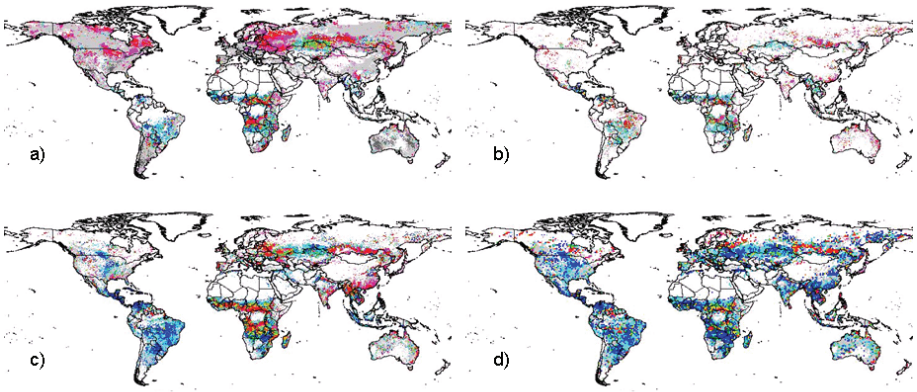

Class	slope	difference	Pearson coeff	Season agreement	Class	slope	difference	Pearson coeff	Season agreement
C1a	$\alpha \leq 30°$	High underestimate	$r > 0.7$	Strong	C3a	$45° < \alpha \leq 60°$	Low overestimate	$r > 0.7$	Strong
C1b			$0.3 < r \leq 0.7$	Weak	C3b			$0.3 < r \leq 0.7$	Weak
C2a	$30° < \alpha \leq 45°$	Low underestimate	$r > 0.7$	Strong	C4a	$60° < \alpha \leq 90°$	High overestimate	$r > 0.7$	Strong
C2b			$0.3 < r \leq 0.7$	Weak	C4b			$0.3 < r \leq 0.7$	Weak

Fig. 3. Categories for the difference between MOPITT and VGT **(a)**, ATSR **(b)**, MODIS **(c)** and GFED2 **(d)** inventories. Color keys are shown in the table at the bottom; no correlation ($-0.3<r<0.3$) and negative correlation ($r<-0.3$) classes are displayed in light and dark grey, respectively.

ACPD
10, 17657–17697, 2010

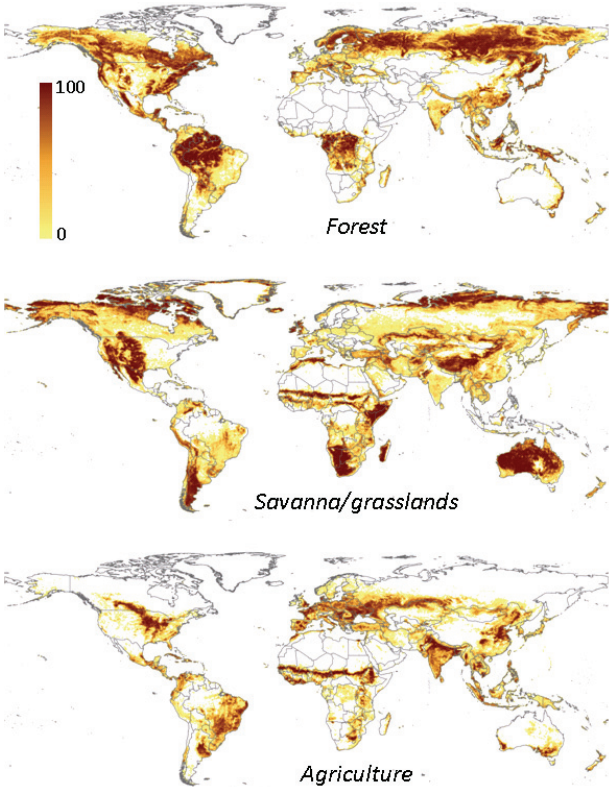

Fig. 4. Proportion of each 0.5×0.5° cell covered by the broad land cover types derived by grouping the GLC2000 classes.

ACPD
10, 17657–17697, 2010

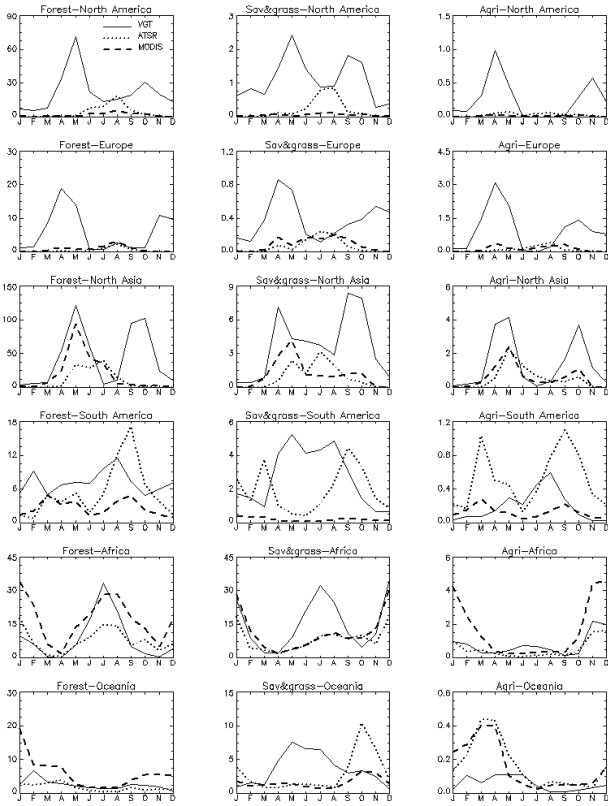

Fig. 5. Seasonality of CO emissions [Tg CO month^{-1}] for the six continental windows and the three macro land cover types (forest, savanna/grassland and agriculture).

ACPD
10, 17657–17697, 2010